Tracking and Data Fusion in Joint Sensing and Communication Networks

# Tracking and Data Fusion in Joint Sensing and Communication Networks

Elia Favarelli,† Elisabetta Matricardi,† Lorenzo Pucci,† Enrico Paolini,† Wen Xu,‡ and Andrea Giorgetti†

†Wireless Communications Laboratory, CNIT, DEI, University of Bologna, Italy
Email: {elia.favarelli, elisabett.matricard3, lorenzo.pucci3, e.paolini, andrea.giorgetti}@unibo.it
‡Munich Research Center, Huawei Technologies Duesseldorf GmbH, Munich, Germany
Email: wen.dr.xu@huawei.com

***Abstract*—In this paper, we consider a beyond-5G multiple-input multiple-output (MIMO) joint sensing and communication (JSC) system where the base stations (BSs) act as monostatic radars by exploiting the signal transmitted to the user equipments (UEs) through a multi-beam radiation pattern. This generates a trade-off between the two functionalities, which should be investigated. This work aims to show the benefits of tracking algorithms to the root mean squared error (RMSE) of an object's position estimation by reserving only a small fraction of the transmitted power for sensing. First, we compare the performance obtained with several tracking algorithms, such as the cubature Kalman filter (CKF), Gaussian mixture cardinalized probability hypothesis density (GMCPHD) and particle filter (PF), by varying the radar cross-section (RCS) of the object and the power devoted to sensing. Then, we consider a scenario where multiple monostatic JSC systems cooperate to improve the target position estimate accuracy via data fusion performed by tracking algorithms. Numerical results show that all tracking methods improve sensing performance under typical wireless communication scenarios and that cooperative sensing through data fusion boosts the whole system's performance significantly, allowing the network designer to save resources for communication.**

## I. Introduction

For the next generation of wireless networks, many emerging functionalities are envisioned, some of which are not simply auxiliary capabilities but essential services. One is the ability to perform sensing via radio frequency (RF) signals enabled by the evolution toward higher frequency bands and larger antenna arrays. Such functionality will support a variety of applications, such as autonomous driving, urban traffic monitoring, assisted living, imaging of a room, and many others [1]. Among the many applications, safety in industrial environments is an emerging area where sensing may represent a technology pillar. In this scenario, the exceptionally high density of internet of things (IoT) devices and base stations (BSs) envisioned in 6G systems paves the way to accurate and reliable localization, e.g., to monitor human-robot cooperation tasks [2]. Furthermore, with the development of mmWave and massive multiple-input multiple-output (MIMO) technology, it has become possible not only to achieve very high capacity links and reduced latencies for communication users through spatial multiplexing but also to perform very accurate direction of arrival (DoA) and direction of departure (DoD) estimation and moving target tracking, to address emerging communication challenges, e.g., beam management [3]. In [4], the authors proposed a predictive beam tracking approach in vehicular scenarios for the extended target case using joint sensing and communication (JSC). Through beam tracking, it is possible to maintain high-quality links by accurately estimating the direction of the desired target [5]. However, to ensure that a system can simultaneously communicate and sense the environment, it is necessary to devote part of its physical and virtual resources to sensing tasks. For these reasons, this work aims to address the analysis of a JSC system to evaluate the key parameters that govern the performance of a data fusion tracking system. In particular, the main contributions are the following:

- We consider a MIMO multibeam JSC system based on orthogonal frequency division multiplexing (OFDM) modulation operating at mmWave, where a fraction of the power is used for the sensing beam.
- We evaluate the performance of three different tracking algorithms, cubature Kalman filter (CKF), particle filter (PF), and Gaussian mixture cardinalized probability hypothesis density (GMCPHD) filter, and we compare their performance with the target positioning error without tracking.
- We analyze the algorithms' dependence on the key parameters (distance $r$, radar cross-section (RCS). $\sigma_{\mathrm{RCS}}$, and fraction of power for sensing $\rho$).
- We propose using tracking algorithms to perform non-linear data fusion, and we compare their performance.

Throughout this paper, capital boldface letters denote matrices, lowercase bold letters indicate vectors, and $\left\|\cdot\right\|_p$ stands for the $p$-norm operator. The paper is organized as follows. In Section II, the monostatic configuration and the proposed JSC system are described. Section III introduces the tracking algorithms and fusion strategies adopted. In Section IV, the performance of tracking and data fusion strategies are evaluated. Conclusions are drawn in Section V.

This work has been carried out in the framework of the CNIT National Laboratory WiLab and the WiLab-Huawei Joint Innovation Center.

978-1-6654-5975-4/22/$31.00 ©2022 IEEE

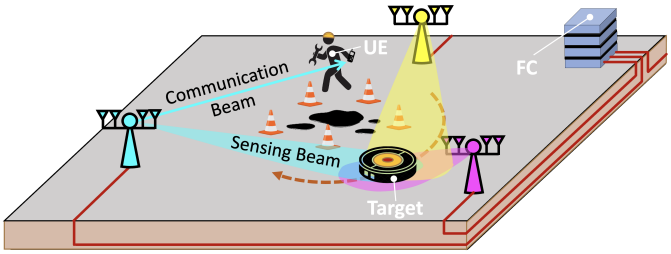


Figure 1: An industrial scenario enabled by a JSC network where multibeam MIMO BSs have monostatic sensing capability and cooperate via data fusion for enhanced target (robot) localization. Data fusion can be performed at the edge by the FC.

## II. System Model and Estimation Techniques

In this work, a JSC network consisting of monostatic MIMO BSs, which cooperate through a fusion center (FC) to perform target localization is considered and depicted in Fig. 1. In the proposed system, each BS consists of a transmitter (Tx) with $N_{\mathrm{T}}$ antenna elements and of a receiver (Rx) with $N_{\mathrm{R}}$ antenna elements belonging to a uniform linear array (ULA), whose elements are equally spaced of half-wavelength, i.e., $d = \lambda/2$ with $\lambda = c/f_{\mathrm{c}}$, where $c$ is the speed of light, and $f_{\mathrm{c}}$ is the carrier frequency. In particular, we consider a multibeam system, where the transmitted signal is used both for communication and sensing, with a communication beam fixed toward the user while the sensing beam tracks the target. The communication system transmits a 5G new radio (NR) waveform with $M$ OFDM symbols and $K$ active subcarriers to a user equipment (UE) in the cell [6].[1] The baseband signal transmitted by the $n$th antenna can be written as

$$b_n(t) = \sum_{m=0}^{M-1} \left( \sum_{k=0}^{K-1} \tilde{x}_{n,k}^{(m)} e^{j2\pi \frac{k}{T} t} \right) u(t - mT_{\mathrm{s}}) \qquad (1)$$

where $\tilde{x}_{n,k}^{(m)}$ is the complex modulation symbol transmitted to the UE in the $m$th OFDM symbol and $k$th subcarrier, mapped through digital precoding, $u(t)$ is the pulse shape, $\Delta f = 1/T$ is the subcarrier spacing, and $T_{\mathrm{s}}$ is the total OFDM symbol duration.

### A. Joint Waveform

Building on our previous works [7], [8], at the Tx, the complex modulation symbols $x_k^{(m)}$ are mapped at each antenna through a digital precoder $\mathbf{w}_{\mathrm{T}} \in \mathbb{C}^{N_{\mathrm{T}} \times 1}$, to obtain the transmitted vector $\tilde{\mathbf{x}}_k^{(m)} = \mathbf{w}_{\mathrm{T}} x_k^{(m)} \in \mathbb{C}^{N_{\mathrm{T}} \times 1}$. In particular, we consider a multibeam system where the power of the signal to be transmitted is split between communication and sensing through a factor $\rho \in [0, 1]$, namely, the total available power is in part exploited to perform radar tasks and in part directed to the UE. Therefore, the transmitting beamformer (BF) vector $\mathbf{w}_{\mathrm{T}}$ can be written as [9]

$$\mathbf{w}_{\mathrm{T}} = \sqrt{\rho}\, \mathbf{w}_{\mathrm{T,s}} + \sqrt{1-\rho}\, \mathbf{w}_{\mathrm{T,c}} \qquad (2)$$

[1]Without loss of generality, we consider one user (e.g., a person) that differs from the targets (e.g., a robot) as depicted in Fig. 1. However, while the sensing beam tracks a target, the UE may change according to the multiple access rule established for communication.

where $\mathbf{w}_{\mathrm{T,c}}$ and $\mathbf{w}_{\mathrm{T,s}}$ are the communication and the sensing BF vectors, respectively. The latter are defined as [6]

$$\mathbf{w}_{\mathrm{T,c}} = \frac{\sqrt{P_{\mathrm{T}} G_{\mathrm{T}}^{\mathrm{a}}}}{N_{\mathrm{T}}} \mathbf{a}_{\mathrm{T}}^{c}(\theta_{\mathrm{T,c}}), \quad \mathbf{w}_{\mathrm{T,s}} = \frac{\sqrt{P_{\mathrm{T}} G_{\mathrm{T}}^{\mathrm{a}}}}{N_{\mathrm{T}}} \mathbf{a}_{\mathrm{T}}^{c}(\theta_{\mathrm{T,s}}) \quad (3)$$

where $G_{\mathrm{T}}^{\mathrm{a}}$ is the transmit array gain along the beam steering direction (where such a gain is maximum), $P_{\mathrm{T}} G_{\mathrm{T}}^{\mathrm{a}}$ is the effective isotropic radiated power (EIRP), $\mathbf{a}_{\mathrm{T}}(\theta_{\mathrm{T,c}}) \in \mathbb{C}^{N_{\mathrm{T}} \times 1}$ and $\mathbf{a}_{\mathrm{T}}(\theta_{\mathrm{T,s}}) \in \mathbb{C}^{N_{\mathrm{T}} \times 1}$ are the steering vectors for communication and sensing, respectively [8].

The sensing system operates in two steps: first, a discovery phase, where the system detects the targets while it is scanning the environment, is performed; then, the second step consists of a tracking phase, where the system is aware of the target position and velocity and can illuminate it with the sensing beam.

The sensing functionality aims at estimating the range, Doppler, and DoA of the target; such estimates will be denoted with the term *measurements* in the following. The system performs measurements with a sampling rate $f_{\mathrm{s}}$ (in measurements per second) and for each sensing direction, a predetermined number of OFDM symbols $M_{\mathrm{s}} < M$ is acquired by the Rx, which will be used for range and speed estimation. The vector $\tilde{\mathbf{y}}_k^{(m)} \in \mathbb{C}^{N_{\mathrm{R}} \times 1}$ of the received symbols at each antenna, after OFDM demodulation, is given by

$$\tilde{\mathbf{y}}_k^{(m)} = \mathbf{H}_k^{(m)} \tilde{\mathbf{x}}_k^{(m)} + \tilde{\mathbf{n}}_k \qquad (4)$$

where $\mathbf{H}_k^{(m)} \in \mathbb{C}^{N_{\mathrm{R}} \times N_{\mathrm{T}}}$ is the channel matrix for the $m$th OFDM symbol and the $k$th subcarrier, and $\tilde{\mathbf{n}}_k \sim \mathcal{CN}(\mathbf{0}, \sigma_{\mathrm{N}}^2 \mathbf{I}_{N_{\mathrm{R}}})$.[2] Considering $L$ point target reflections, the channel matrix can be written as

$$\mathbf{H}_k^{(m)} = \sum_{l=1}^{L} \alpha_l e^{j2\pi m T_{\mathrm{s}} f_{\mathrm{D},l}} e^{-j2\pi k \Delta f \tau_l} \mathbf{a}_{\mathrm{R}}(\theta_l) \mathbf{a}_{\mathrm{T}}^{T}(\theta_l) \qquad (5)$$

where $\tau_l$, $f_{\mathrm{D},l}$, $\theta_l$, and $\mathbf{a}_{\mathrm{R}}(\theta_l)$ are the round-trip delay, the Doppler shift, the DoA, and the array response vector at the receiver for sensing of the $l$th target, respectively. The complex amplitude $\alpha_l = |\alpha_l| e^{j\phi_l}$ in (5) includes phase shift and attenuation along the $l$th propagation path. Starting from (4), by performing spatial combining through the receiving BF vector, $\mathbf{w}_{\mathrm{R}} = \mathbf{a}_{\mathrm{R}}^{c}(\theta_{\mathrm{R,s}})$, we have the received symbols $y_k^{(m)} = \mathbf{w}_{\mathrm{R}}^{T} \tilde{\mathbf{y}}_k^{(m)}$. The OFDM symbols collected in each direction are used to estimate range, Doppler, and DoA of the target.

### B. Sensor-Target-Sensor Path

DoA, range, and velocity estimates depend on the signal-to-noise ratio (SNR) at the Rx. In line-of-sight (LOS) propagation conditions, at a given array element from the $l$th path illuminated by the sensing beam, the SNR can be defined as

$$\mathrm{SNR}_l = \rho \cdot \gamma_l \cdot \frac{P_{\mathrm{T}} G_{\mathrm{T}}^{\mathrm{a}} G_{\mathrm{R}} c^2 \sigma_{\mathrm{RCS},l}}{(4\pi)^3 f_{\mathrm{c}}^2 d_l^4 N_0 K \Delta f} \qquad (6)$$

[2]We do not consider self-interference due to imperfect TX–RX isolation as this aspect is out of the paper scope.

where $d_l$ is the distance of the $l$th point target, with RCS $\sigma_{\mathrm{RCS},l}$, from the BS, $G_{\mathrm{R}}$ is the single element antenna gain at the Rx, $N_0$ is the one-sided noise power spectral density (PSD) at each antenna element, and $\gamma_l = |\mathrm{AF}(\theta_{\mathrm{T,s}} - \theta_l)|^2 \in [0,1]$. The normalized array factor at the Tx, $\mathrm{AF}(\theta)$, is taken into account to consider the imperfect alignment between the target DoA and the sensing direction; when $\theta_l = \theta_{\mathrm{T,s}}$ then $\gamma_l = 1$. When convenient, by normalizing the received symbols after the fast Fourier transform (FFT) in the OFDM receiver to unit power, (6) reduces to $\mathrm{SNR}_l = 1/\sigma_{\mathrm{N}}^2$.

### C. Measurements Performed by Monostatic Sensors

The estimation methods are performed for each sensing direction in which $M_{\mathrm{s}}$ OFDM symbols are collected. Starting from the vector of the received symbols $\tilde{\mathbf{y}}_k^{(m)}$, MUltiple SIgnal Classification (MUSIC) is performed to obtain the DoA estimate. Furthermore, for the range-Doppler profile evaluation, first, starting from the received symbols obtained after spatial combining, a division is performed to remove the unwanted data symbols [10], i.e., $u_k^{(m)} = y_k^{(m)}/x_k^{(m)}$. Note that $u_k^{(m)}$ contains, for each target, two complex sinusoids whose frequencies are related to $f_{\mathrm{D},l}$ and $\tau_l$. Next, a periodogram can be computed to estimate range and speed of the target as [10], [11]. This periodogram represents the range-Doppler map where distance and velocity resolutions depend on the 5G NR parameters, i.e., number of OFDM symbols, number of active subcarriers, subcarrier spacing, and OFDM symbol duration.

In this paper, we consider the position estimation extracted by the sensors using DoA and range, ignoring the velocity. The range resolution provided by the system is thus [10]

$$\Delta r = \frac{c}{2\Delta f K_{\mathrm{p}}} \tag{7}$$

with $K_{\mathrm{p}}$ the smallest power of two greater than $K$.

Without loss of generality, in the following we focus on one target (different from the UE), hence $L = 1$.

## III. Tracking Algorithms and Data Fusion

This section provides a brief review of the algorithms used for target tracking. Over the years, several algorithms have been proposed to address the tracking task [12]–[16]. Bayesian filtering theory is one of the most successful approaches to implementing target tracking. This framework is based on predicting the target state probability density function (p.d.f.) in a time instant $t$ from that at the instant $t-1$, and updating the predicted distribution with the measurements collected at the time instant $t$:

$$p_{t-1}(\mathbf{s}_{t-1}|\mathbf{Z}_{1:t-1}) \rightarrow p_{t|t-1}(\mathbf{s}_t|\mathbf{Z}_{1:t-1}) \rightarrow p_t(\mathbf{s}_t|\mathbf{Z}_{1:t})$$

where $\mathbf{s}_t$ stands for the target state vector at the instant $t$, $\mathbf{Z}_{1:t-1}$ represent the set of measurements acquired from the instant 1 to the instant $t-1$, and $p(\cdot)$ stands for the p.d.f. function. Prior and posterior distributions derived with the Bayesian approach [12], [17] assume the following form:

$$p_{t|t-1}(\mathbf{s}_t|\mathbf{Z}_{1:t-1}) = \int f_{t|t-1}(\mathbf{s}_t|\mathbf{s}) p_{t-1}(\mathbf{s}|\mathbf{Z}_{1:t-1})\, d\mathbf{s} \tag{8}$$

$$p_t(\mathbf{s}_t|\mathbf{Z}_{1:t}) = \frac{g_t(\mathbf{Z}_t|\mathbf{s}_t) p_{t|t-1}(\mathbf{s}_t|\mathbf{Z}_{1:t-1})}{\int g_t(\mathbf{Z}_t|\mathbf{s}) p_{t:t-1}(\mathbf{s}|\mathbf{Z}_{1:t-1})\, d\mathbf{s}} \tag{9}$$

where $f_{t|t-1}(\mathbf{s}_t|\mathbf{s})$ stands for the process model, and $g_t(\mathbf{Z}_t|\mathbf{s})$ represents the measurement model. In a large set of problems, measurement and process models are described by non-linear transformations, the noise has a non-Gaussian distribution, and prior and posterior have complex distributions to track. For these reasons, three different strategies to handle such an issue are considered in the following, namely CKF, PF, and GMCPHD filter.

### A. Cubature Kalman Filter

In this solution, the prior distribution is sampled in some predefined positions (sigma points), which are then propagated with the prediction and update equations. Subsequently, the mean and covariance of the sigma points are evaluated, and the posterior is approximated with a Gaussian distribution with the estimated mean and covariance [18]–[20]. In CKF the sigma points are selected as

$$\boldsymbol{\xi}_t^{(i)} = \hat{\mathbf{s}}_t + \sqrt{D}\,(\mathbf{P}_t^{\frac{1}{2}})_i, \quad \boldsymbol{\xi}_t^{(i+D)} = \hat{\mathbf{s}}_t - \sqrt{D}\,(\mathbf{P}_t^{\frac{1}{2}})_i \tag{10}$$

where $\boldsymbol{\xi}_t^{(i)}$ is the $i$th sigma point (with $i \in [1, D]$ with step of 1), $\hat{\mathbf{s}}_t$ is the expected value of the random variable $\mathbf{s}_t$, $D$ is the distribution dimensionality and $\mathbf{P}_t$ is the covariance matrix of $\mathbf{s}_t$.[3] All the sigma points are equally weighted, with weights $w_i = \frac{1}{2D}$. The main advantage of this technique is the absence of hyper-parameters to set. However, growing the dimensionality, the sigma points diverge from the mean value of the distribution, increasing the estimation error. Moreover, sigma points methods cannot handle strong non-linearity in the sampled distribution. To implement data fusion with CKF, we modified the measurement equation to hold a set of measurements coming from different sensors and map them in the state vector.

### B. Particle Filter

Through this approach, the target state distribution is estimated with a set of weighted particles. Each particle is then propagated to the next step with the process equation and updated with the measurement equation [21], [22]. In this case, the posterior distribution $p_t(\mathbf{s}_t|\mathbf{Z}_t)$ is approximated by

$$p_t(\mathbf{s}_t|\mathbf{Z}_t) = \sum_{q=1}^{N_{\mathrm{p}}} w_t^{(q)} \delta(\mathbf{s}_t - \mathbf{s}_t^{(q)}) \tag{11}$$

where $N_{\mathrm{p}}$ represent the number of particles, $t$ and $q$ are the time and particle index respectively, $w_t^{(q)}$ is the $q$th particle weight at time $t$, and $\delta(\mathbf{s}_t - \mathbf{s}_t^{(q)})$ is a delta function centred in the particle coordinates $\mathbf{s}_t^{(q)}$. The particles weights $w_t^{(q)}$ have the scope to handle the measurement model behaviour, and are updated as follows:

$$w_t^{(q)} = w_{t-1}^{(q)} g_t(\mathbf{Z}_t|\mathbf{s}_t). \tag{12}$$

[3] $(\mathbf{P}_t^{\frac{1}{2}})_i$ represent the $i$th column of the matrix $\mathbf{P}_t^{\frac{1}{2}}$.

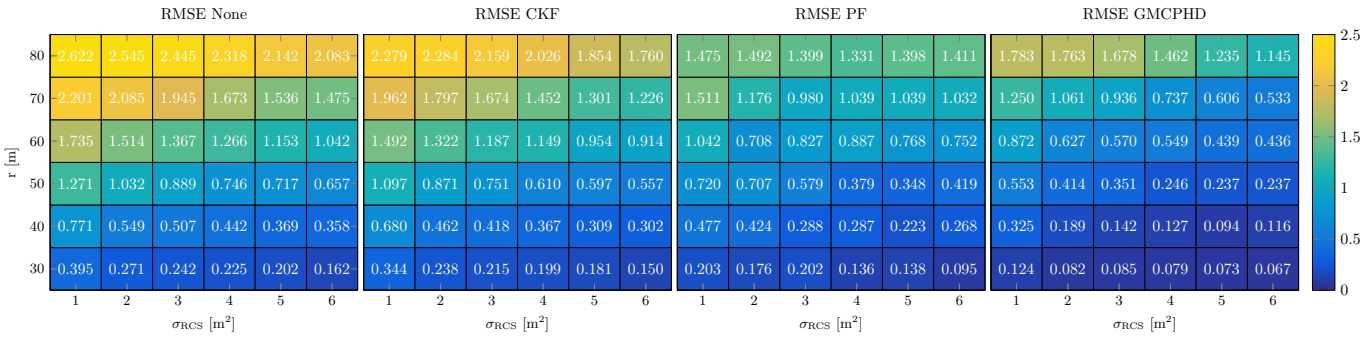


Figure 2: Tracking algorithm performance, varying the distance $r$ and the radar cross-section $\sigma_{\mathrm{RCS}}$, with fraction of power $\rho = 0.1$.

The algorithm proceeds updating the particle position with the process model equation and the weights with the measurement model equation. To prevent weights drift, the sequential importance re-sampling strategy is implemented, setting all the weights to $w_t^{(q)} = \frac{1}{N_{\mathrm{p}}}$ when the number of effective particles $N_{\mathrm{e}} = 1/\sum_{q=1}^{N_{\mathrm{p}}} \left(w_t^{(q)}\right)^2$ goes below a certain threshold $N_{\mathrm{e}}^{(\min)}$. This strategy usually presents better accuracy by increasing the number of particles at the cost of computational complexity. The particle weights are updated with measurements from all sensors in the data fusion setup.

### C. Gaussian Mixture Probability Hypothesis Density Filter

In this case, the prior and posterior distributions are approximated with a Gaussian mixture [23], i.e., a weighted sum of Gaussian functions as

$$p_t(\mathbf{s}_t|\mathbf{Z}_t) = \sum_{r=1}^{\mathcal{M}} w_r \mathcal{N}(\boldsymbol{\mu}_r, \boldsymbol{\Sigma}_r) \tag{13}$$

where $w_r$ is the $r$th weight, and $\mathcal{N}(\boldsymbol{\mu}_r, \boldsymbol{\Sigma}_r)$ the $i$th Gaussian distribution with mean value $\boldsymbol{\mu}_r$ and covariance $\boldsymbol{\Sigma}_r$. Each Gaussian function is then propagated to the next step and updated with the measurement equation. The GMCPHD filter also propagates the cardinality of the targets, resulting in a more stable estimation of the number of targets. This strategy represents a flexible tool that usually presents high accuracy in a wide set of tracking problems [14]. The principal parameters involved in the filter are the following: $\mathcal{M}$ is the Gaussian mixture order, $C_{(\max)}$ stands for the maximum targets set cardinality detectable, $\nu$ and $\zeta$ represent the pruning and merging thresholds respectively, and $P_{\mathrm{D}}$ and $P_{\mathrm{S}}$ stand for the detection and survival probability, respectively. The main issues with this approach are the model's linearization (which increases the error when the target or sensor behaviors are strongly non-linear) and the wide set of parameters. To implement data fusion with GMCPHD with a single target it is enough to force $C_{(\max)} = 1$, in order to evaluate the most likely target position among all the possible hypotheses.

## IV. Numerical Results

In this section, two different scenarios are evaluated. Firstly, we consider a single JSC monostatic sensor with a target (object) moving on a circumference at a fixed distance from the sensor. A 5G NR signal compliant with 3GPP Technical Specification in [24] is considered. The system operates with $f_{\mathrm{c}} = 28\,\mathrm{GHz}$, with subcarrier spacing $\Delta f = 120\,\mathrm{kHz}$, bandwidth equal to $400\,\mathrm{MHz}$, $N_{\mathrm{T}} = N_{\mathrm{R}} = 50$ antennas (which corresponds to a beamwidth equal to $5.3°$), the EIRP is set to $43\,\mathrm{dBm}$, and the noise PSD is $N_0 = 4 \cdot 10^{-20}\,\mathrm{W/Hz}$. For each sensing direction, $K = 3168$ active subcarriers and $M_{\mathrm{s}} = 112$ OFDM symbols are acquired out of the $M = 1120$ symbols of the 5G frame. The RCS is modeled according to a Swerling I distribution with mean value $\sigma_{\mathrm{RCS}}$, which is varied in the range $\sigma_{\mathrm{RCS}} \in [1,\, 6]\,\mathrm{m}^2$ (with $1\,\mathrm{m}^2$ step). The radius of the object trajectory varies in the range $r \in [30,\, 80]\,\mathrm{m}$ with $10\,\mathrm{m}$ step, to evaluate the performance at different distances, with a constant tangential velocity of $v = 12\,\mathrm{m/s}$. The sensor collects measurements (range and angle) at a rate $f_s = 100\,\mathrm{Hz}$ and the number of measurement acquired along the trajectory is $\mathcal{K} = 500$. The system is tested with two different values of the fraction of transmit power devoted to sensing, i.e., $\rho \in [0.1,\, 0.5]$. Secondly, the algorithms are tested in a data fusion setting, where measurements are gathered by 3 sensors ($S_1$, $S_2$, $S_3$), and fused by the algorithms, as described in Section III, to enhance the sensing performance. In this scenario, depicted in Fig. 4a, the target starts from the position $(12.50, 21.65)\,\mathrm{m}$ highlighted with a black dot, and moves accordingly to a clockwise circular uniform motion, with tangential velocity $v = 12\,\mathrm{m/s}$ and radius $r = 25\,\mathrm{m}$. The monostatic sensors are represented with colored squares, and measurements related to each sensor are reported with dots of the same color. The ground truth trajectory is reported in black. In this case the mean RCS $\sigma_{\mathrm{RCS}} = 1\,\mathrm{m}^2$, and power fraction $\rho = 0.1$ are fixed. The sensor has a sampling rate $f_s = 100\,\mathrm{Hz}$ and the number of measurement acquired is $\mathcal{K} = 1300$. The sensing performance is evaluated by the root mean squared error $\mathrm{RMSE} = \left(\sum_{t=1}^{\widehat{\mathcal{K}}} \left\|\mathbf{s}_t - \tilde{\mathbf{s}}_t\right\|_2^2 / \widehat{\mathcal{K}}\right)^{1/2}$ where $\widehat{\mathcal{K}}$ is the number of measurement considered, and $\mathbf{s}_t$ and $\tilde{\mathbf{s}}_t$ are the true and estimated target states at the time instant $t$, respectively. In Fig.4b, to evaluate the root mean squared error (RMSE) evolution over the time, we consider the last $\widehat{\mathcal{K}} = 20$ measurements.

For all the algorithms, the state vector dimensionality is

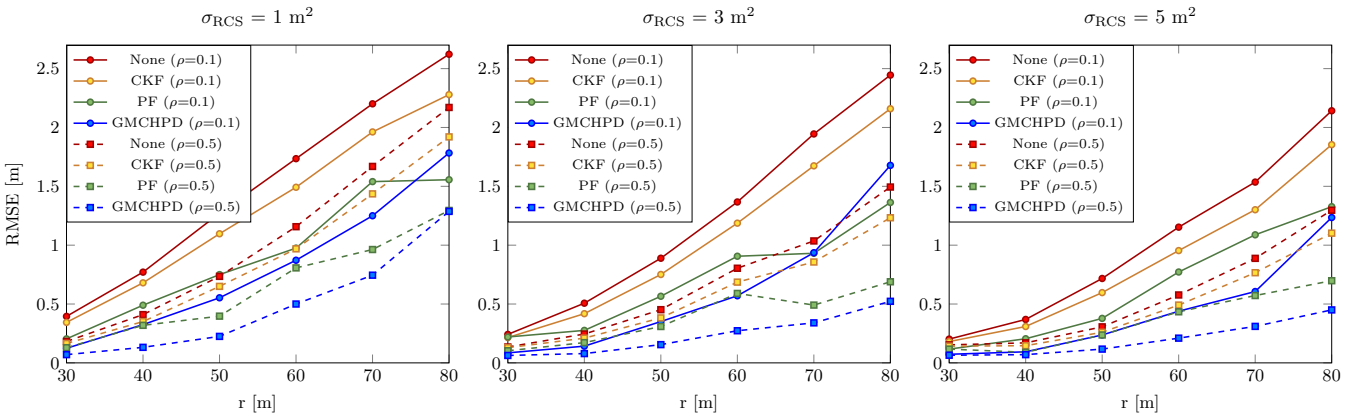


Figure 3: Tracking algorithm performance, varying the distance $r$, the fraction of power $\rho$, and the radar cross-section $\sigma_{\mathrm{RCS}}$.

$D = 2$, the measurement noise covariance matrix $\mathbf{R} = \mathrm{diag}(0.5, 0.5)\,\mathrm{m}^2$, and the process noise covariance matrix $\mathbf{Q} = \mathrm{diag}(0.01, 0.01)\,\mathrm{m}^2$. These covariance matrices reflect the simulated measurement error and the target model in the specific scenario and parameters setting. In the measurement model we considered to directly evaluate the target position, and for the process model we use a constant velocity model. In the PF, the number of particles is $N_{\mathrm{p}} = 1000$ and the minimum number of effective particle is $N_{\mathrm{e}}^{(\mathrm{min})} = 600$. In the GMCPHD filter, the probability of detection is $P_{\mathrm{D}} = 0.99$, the probability of survival is $P_{\mathrm{S}} = 0.99$, the maximum Gaussian order $\mathcal{M}$ is set equal to 100, the maximum cardinality $C_{(\mathrm{max})}$ is set to 1, pruning and merging thresholds are $\nu = 3$ and $\zeta = 10^{-5}$, respectively.

### A. Impact of Range and Radar Cross-Section

In this section, we analyze the impact of the distance between target and sensor and the target RCS, which affect the SNR of the signal received by the sensor. In Fig. 2, the RMSE error varying the distance $r$, the mean RCS $\sigma_{\mathrm{RCS}}$ and the tracking algorithm adopted, is reported for $\rho = 0.1$. All tracking algorithms are beneficial in reducing the RMSE of target position estimation, especially in harsh conditions, i.e., when $r$ is larger than 50 m or the mean RCS $\sigma_{\mathrm{RCS}}$ is smaller than $4\,\mathrm{m}^2$. The algorithms that exhibit the highest performance are the GMCPHD filter and the PF. The first one presents the best performance on average, but the PF achieves lower RMSE when the conditions are extremely unfavorable; this is due to its capability to handle non-linear dependencies in the posterior distribution.

### B. Sensing/Communications Trade-off via $\rho$

To highlight the influence of the fraction of power $\rho$ on the sensing performance, Fig. 3 shows the RMSE of position estimation with $\rho = 0.1$ (solid curves), and $\rho = 0.5$ (dashed curves). The average RCS $\sigma_{\mathrm{RCS}}$ is also varied between $1\,\mathrm{m}^2$ to $5\,\mathrm{m}^2$. As it can be seen, in the most challenging scenario where the fraction of power $\rho$ is low, e.g., $\rho = 0.1$, tracking algorithms can significantly increase the sensing range and the sensing capability to localize weak targets. Also, from Fig. 3 it is possible to appreciate that GMCPHD filter has the best performance in general, but PF performs better in a scenario with low SNR of the target (6). For example, when $\sigma_{\mathrm{RCS}} = 1\,\mathrm{m}^2$ and $\rho = 0.1$ the RMSE is 1 m at $r = 44\,\mathrm{m}$ without tracking, and at 63 m with GMCPHD tracking with a significant increase of 43% of sensing range. On the communication side, the theoretical spectral efficiency is $\eta = \log_2(1 + (1-\rho)\mathrm{SNR}^{\mathrm{c}})$, where $\mathrm{SNR}^{\mathrm{c}}$ represents the communication SNR when $\rho = 0$, i.e., when the overall transmit power is reserved for communication. Hence, for $\mathrm{SNR}^{\mathrm{c}} = 10\,\mathrm{dB}$, the spectral efficiency is $\eta = 3.32\,\mathrm{bit/s/Hz}$ when $\rho = 0.1$, while increasing $\rho$ to 0.5, the spectral efficiency reduces by 22% to $\eta = 2.59\,\mathrm{bit/s/Hz}$.

### C. Data Fusion from Multiple Monostatic Sensors

In the multi-sensor scenario reported in Fig. 4a, we focused on the performance evaluation of the tracking algorithms when used for data fusion as presented in Section III. Fig. 4 shows the RMSE evolution over time, i.e., along the trajectory. As a benchmark, the mean track reported in red is evaluated by averaging the measurements gathered by the 3 monostatic sensors and evaluating the RMSE between them and the ground truth. As we can see, CKF reduces the RMSE with respect to the benchmark strategy, but the performance of PF and GMCPHD filter produce much better results. The oscillation particularly present in the PF is due to the approximation of the measurement model; they can be reduced by increasing process noise but at the expense of lower accuracy. In Fig. 4c, the performance of the algorithms is evaluated considering the measurements from only one sensor at a time (cyan, magenta, and yellow bars) and compared with the performance obtained by fusing the data from the 3 sensors (green bar). It can be noticed that data fusion leads to a considerable performance improvement, which results in a RMSE reduction by a factor of 3 when using the PF and 4 when using the cardinalized probability hypothesis density (CPHD) filter.

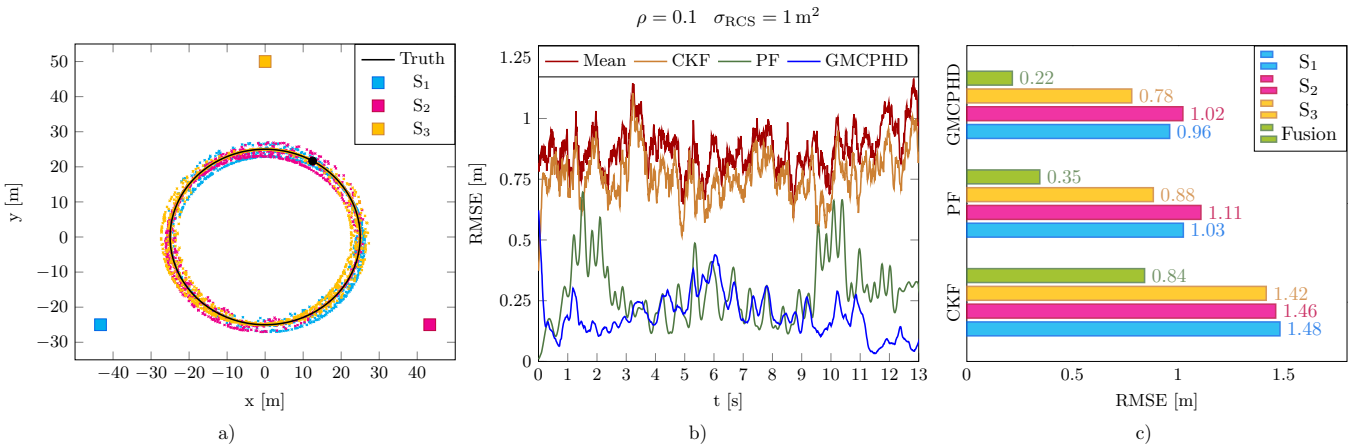


Figure 4: a) Scenario configuration. b) RMSE evolution over the time. c) RMSE with single sensors and data-fusion solutions.

## V. Conclusion

This work presented the investigation of the benefit of tracking algorithms to reduce the estimation error in a beyond-5G JSC system with monostatic sensing. Tracking is also used as a means of non-linear data fusion when the target is visible from multiple BSs. The performance is evaluated in different scenarios varying the target RCS, the target distance to the BS, and the fraction of power adopted for sensing. Numerical results show that GMCPHD leads to very good performance in general, but PF exhibits better performance in scenarios with reduced SNR. Finally, it is shown that fusing data from a set of sensors allows for achieving better performance than the scenario with a single sensor, emphasizing the network's vital role in collecting measurements in a distributed manner.

## References


[1] F. Liu, Y. Cui, C. Masouros, J. Xu, T. X. Han, Y. C. Eldar, and S. Buzzi, "Integrated sensing and communications: Towards dual-functional wireless networks for 6g and beyond," *IEEE J. Sel. Areas Commun.*, vol. 40, pp. 1728–1767, 2022.

[2] Z. Feng, Z. Wei, X. Chen, H. Yang, Q. Zhang, and P. Zhang, "Joint communication, sensing, and computation enabled 6G intelligent machine system," *IEEE Network*, vol. 35, no. 6, pp. 34–42, 2021.

[3] Y. Cui, F. Liu, X. Jing, and J. Mu, "Integrating sensing and communications for ubiquitous IoT: Applications, trends, and challenges," *IEEE Network*, vol. 35, pp. 158–167, 2021.

[4] Z. Du, F. Liu, and Z. Zhang, "Sensing-assisted beam tracking in V2I networks: Extended target case," in *ICASSP 2022 - 2022 IEEE International Conference on Acoustics, Speech and Signal Processing (ICASSP)*, 2022, pp. 8727–8731.

[5] F. Liu, P. Zhao, and Z. Wang, "EKF-based beam tracking for mmwave mimo systems," *IEEE Commun. Lett.*, vol. 23, no. 12, pp. 2390–2393, 2019.

[6] H. Asplund, D. Astely, P. von Butovitsch, T. Chapman, M. Frenne, F. Ghasemzadeh, M. Hagström, B. Hogan, G. Jöngren, J. Karlsson *et al.*, *Advanced Antenna Systems for 5G Network Deployments: Bridging the Gap Between Theory and Practice*. Academic Press, 2020.

[7] L. Pucci, E. Matricardi, E. Paolini, W. Xu, and A. Giorgetti, "Performance analysis of joint sensing and communication based on 5G New Radio," in *IEEE Work. on Adv. in Netw. Loc. and Nav. (ANLN), Globecom 2021*, Madrid, Spain, Dec. 2021.

[8] L. Pucci, E. Paolini, and A. Giorgetti, "System-level analysis of joint sensing and communication based on 5G new radio," in *IEEE J. Sel. Areas Commun.*, vol. 40, no. 7, July 2022, pp. 2043–2055.

[9] J. A. Zhang, X. Huang, Y. J. Guo, J. Yuan, and R. W. Heath, "Multibeam for joint communication and radar sensing using steerable analog antenna arrays," *IEEE Trans. Veh. Technol.*, vol. 68, no. 1, pp. 671–685, Jan. 2019.

[10] M. Braun, "OFDM radar algorithms in mobile communication networks," Ph.D. dissertation, Karlsruhe Institute of Technology, 2014.

[11] C. B. Barneto, T. Riihonen, M. Turunen, L. Anttila, M. Fleischer, K. Stadius, J. Ryynänen, and M. Valkama, "Full-duplex OFDM radar with LTE and 5G NR waveforms: challenges, solutions, and measurements," *IEEE Trans. Microw. Theory Tech.*, vol. 67, no. 10, pp. 4042–4054, Oct. 2019.

[12] R. P. Mahler, *Statistical multisource-multitarget information fusion*. Artech House Norwood, MA, USA, 2007, vol. 685.

[13] B.-T. Vo, B.-N. Vo, and A. Cantoni, "Analytic implementations of the cardinalized probability hypothesis density filter," *IEEE Trans. Signal Process.*, vol. 55, no. 7, pp. 3553–3567, 2007.

[14] B.-N. Vo and W.-K. Ma, "The Gaussian mixture probability hypothesis density filter," *IEEE Trans. Signal Process.*, vol. 54, no. 11, pp. 4091–4104, 2006.

[15] R. Mahler, "PHD filters of higher order in target number," *IEEE Trans. Aerosp. Electron. Syst.*, vol. 43, no. 4, pp. 1523–1543, 2007.

[16] ——, "Multitarget bayes filtering via first-order multitarget moments," *IEEE Trans. Aerosp. Electron. Syst.*, vol. 39, no. 4, pp. 1152–1178, 2003.

[17] S. Särkkä, *Bayesian filtering and smoothing*. Cambridge university press, 2013, no. 3.

[18] S. Haykin and I. Arasaratnam, "Cubature Kalman filters," *IEEE Trans. Autom. Control*, vol. 54, no. 6, pp. 1254–1269, 2009.

[19] B. Jia, M. Xin, and Y. Cheng, "High-degree cubature Kalman filter," *Automatica*, vol. 49, no. 2, pp. 510–518, 2013.

[20] I. Arasaratnam, S. Haykin, and T. R. Hurd, "Cubature kalman filtering for continuous-discrete systems: theory and simulations," *IEEE Trans. Signal Process.*, vol. 58, no. 10, pp. 4977–4993, 2010.

[21] P. Djuric, J. Kotecha, J. Zhang, Y. Huang, T. Ghirmai, M. Bugallo, and J. Miguez, "Particle filtering," *IEEE Signal Process. Mag.*, vol. 20, no. 5, pp. 19–38, 2003.

[22] M. Bolić, P. M. Djurić, and S. Hong, "Resampling algorithms for particle filters: A computational complexity perspective," *EURASIP Journal on Advances in Signal Processing*, vol. 2004, no. 15, pp. 1–11, 2004.

[23] B.-T. Vo, B.-N. Vo, and A. Cantoni, "Analytic implementations of the cardinalized probability hypothesis density filter," *IEEE Trans. Signal Process.*, vol. 55, no. 7, pp. 3553–3567, 2007.

[24] *5G; NR; Physical channels and modulation*, 3GPP TS 38.211, 7 2020, version 16.2.0 Release 16.